Mon. Not. R. Astron. Soc. **282,** 1203–1210 (1996)

IRAS 04210+0400: modelling the optical spectra from flaring large-scale jets

W. Steffen,[1] A. J. Holloway[1] and A. Pedlar[2]
[1]*Department of Astronomy, University of Manchester, Schuster Laboratory, Oxford Road, Manchester M13 9PL*
[2]*Nuffield Radio Astronomy Laboratories, University of Manchester, Jodrell Bank, Macclesfield, Cheshire SK11 9DL*

Accepted 1996 June 2. Received 1996 May 10; in original form 1995 December 7

ABSTRACT

The emission lines in the active galaxy IRAS 04210+0400 show a dramatic (~900 km s^{-1}) increase in the velocity spread at the position of radio hotspots which are located at the beginning of extended radio lobes. We study a simple geometric model of an opening outflow which reproduces the structure found in the long-slit emission-line spectrum of the hotspot regions. The predicted bifurcations in the optical image structure of these regions are confirmed by deep [O III] 5007-Å line imaging. We propose that this phenomenon is the result of a jet emerging from the galaxy through the boundary between the interstellar and intergalactic media. A similar model has previously been suggested as an explanation for wide-angle-tail radio sources (WATs). If our model proves to be correct in more detailed future observations, then IRAS 04210+0400 provides the unique possibility of studying the flaring jet phenomenon at optical wavelengths.

Key words: galaxies: active – galaxies: individual: IRAS 04210+0400 – galaxies: jets – galaxies: kinematics and dynamics – galaxies: Seyfert.

1 INTRODUCTION

Jets in Fanaroff–Riley type I (FR I) radio galaxies can flare very abruptly and show very large opening angles of up to 90° in diffuse lobes or tails (O'Donoghue, Eilek & Owen 1993). These structures often bend near the flaring point. Norman, Burns & Sulkanen (1988) and Loken et al. (1995) have modelled this phenomenon in wide-angle-tail radio galaxies (WATs) in terms of a supersonic jet passing through a shock in the ambient gas where the jet flow becomes subsonic. The jet is then disrupted and entrains external gas, which becomes turbulent with the formation of large- and small-scale eddies. Such a shock in the ambient medium could be due to a supersonic galactic wind moving into the surrounding intergalactic medium.

In order to obtain direct kinematic information, Owen, O'Dea & Keel (1990) conducted a search for optical line emission from the flaring regions in WAT sources but found no significant emission from the five objects they studied. In Holloway et al. (1996, Paper I) we first proposed that a phenomenon similar to the WATs could apply to IRAS 04210+0400 for which optical information is available in the flaring region (Beichman et al. 1985; Hill et al. 1988; Paper I). If our interpretation is correct, then IRAS 04210+0400 is an important test object, allowing us to study such a transition region in the optical regime, thereby providing important kinematic information from spatially resolved spectra.

The active galaxy IRAS 04210+0400 was discovered on scans of the *Infrared Astronomical Satellite* (*IRAS*) by Soifer et al. (1984). Beichman et al. (1985) identified the *IRAS* source with a spiral galaxy at a redshift of $z = 0.046$. Their spectroscopic work revealed the Seyfert 2 type emission-line nucleus of the 16.3 mag (R band) object. First observations with the Very Large Array (VLA) showed an unusual radio structure, consisting mainly of large symmetrically bent lobes (~25 kpc), which seemed to extend the spiral structure beyond the optically detected image (Beichman et al. 1985). Hill et al. (1988) reported the discovery of a central double radio source (~1-arsec separation) and that the lobes start at hotspots which are coincident with anomalous spectral features (Steffen et al. 1996a). Hill et al. found that at the position of the hotspot the spectral lines consisted mainly of an asymmetric narrow (FWHM = 160 km s^{-1}) and a broad (FWHM = 730 km s^{-1}) component. They argued that the extended spiral features found in this galaxy are the photoionized remnants of earlier radio jet activity. Steffen, Holloway & Pedlar (1996b) examined this model in some detail and concluded that it was not consistent with the observations, and suggested an alternative model based on the bending of the jets by the interaction with the rotating interstellar medium.

In Paper I we identified broad red- and blueshifted velocity components (north and south of the continuum peak, respectively) with a spatial separation similar to that of the central double radio source. We spatially resolved the broad spectral features near the radio hotspots and presented first results from a model which explains the spectra as a consequence of an opening cone starting at the radio hotspots. As pointed out in Paper I, the origin of these structures seems to be related to the flaring of the radio structure into extended lobes.

Hubble Space Telescope (*HST*) observations of IRAS 04210+0400 presented by Capetti et al. (1996) spatially resolve the central region into a complex structure with discrete emission-line clouds. There are three particularly bright knots, confirming the triple structure deduced in Paper I from spectroscopic observations. Capetti et al. (1996) also find filamentary high-ionization line emission (coincident with the previously known spiral features) which bifurcates close to the southern radio hotspot. This strongly supports the model proposed in Paper I involving a flaring jet at this position.

In the present paper, we give a more detailed account of the model first proposed in Paper I. In Section 2 we introduce the model, discussing the dependence of the spectral lineshape on the orientation of the outflow with respect to the observer and the direction of the spectrometer slit. In Section 3 we compare our model with the observations. In the same section a new deep emission-line image is presented. We discuss and summarize our results in Sections 4 and 5, respectively.

2 THE MODEL

In this section we describe a simple model which is intended to provide some insight into the existing gross emissivity and flow distribution in the emission-line gas associated with the extended radio emission in IRAS 04210+0400. We model the long-slit spectra using a simple parametrized description of the emissivity and the velocity field of the ionized gas flow. In our model we regard the extended emission-line source around the radio hotspots as a collimated outflow which flares when passing through the boundary between the interstellar medium (ISM) and the intergalactic medium (IGM) (see Fig. 1).

First we give details about the parametrization used in this model. We then discuss the general properties of the predicted images and spectra as a function of orientation in space. After discussing the observational constraints, we present a simple axisymmetric and an improved non-axisymmetric solution which match the observations in some detail.

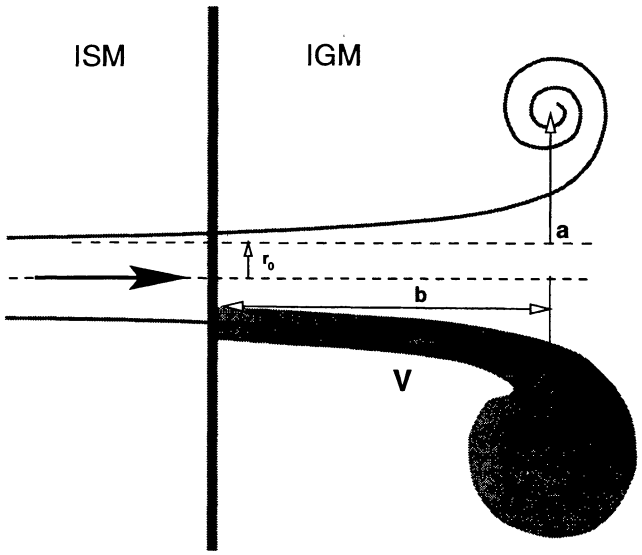

Figure 1. In this line drawing the geometric model parameters of the flow are illustrated. They are the initial radius of the circular cross-section r_0, the distance b of the eddy from the transition region, where the emission is assumed to start, and the distance $r_0 + a$ from the axis.

2.1 Parametrization of the model

Hydrodynamic simulations (Loken et al. 1995) suggest that large-scale eddies often develop in the flaring regions of jets crossing an external shock. They can approximately be described by a circular or spiralling sheet with flow velocities comparable to those of the boundaries of the flaring jet region. For simplicity we parametrize this flow as a hyperbolic spiral given by

$$z'_{(s)} = -\frac{a}{s}\cos(s) + \frac{a}{s_0}\cos(s_0), \tag{1}$$

$$r_{(s)} = \{r_0 + a[1 - \sin(s)/s]\}/\epsilon, \tag{2}$$

$$\epsilon = [1 - e\cos(\phi)]/(1 - e). \tag{3}$$

Here (z',r,ϕ) are cylindrical coordinates, and s is a normalized position parameter along the spiral [with $s_0 = -b/a + \sqrt{2 + (b/a)^2}$]. The parameter r_0 is the initial radial distance from the axis, while ϵ allows for an elliptic cross-section of eccentricity e as a simple approximation to non-axisymmetry. The distance between the centre of the eddy and the axis is given by $r_0 + a$. The parameters a and b are as indicated in Fig. 1. The orientation of the outflow in space is determined by the Euler angles (Θ,Φ,Ψ) with the conventions given in Goldstein (1980).

The calculations are performed on a regular three-dimensional Cartesian grid (x,y,z), with the z-axis along the line of sight. The z-axis of the Cartesian coordinate system coincides with the z'-axis of the cylindrical system used for the representation of the outflow in equations (2) and (3) when the Euler angle $\Theta = 0$. Typical array sizes of the calculations presented here are 80–100 pixel (≈ 10 pixel per arcsec) along a side of the cubic domain. Since we are considering mainly forbidden lines ([O III] 5007 Å and [N II] 6584 Å), the emission is assumed to be optically thin. The image intensity is therefore calculated by adding the emissivity in each pixel along the line of sight.

2.2 Dependence of the spectrum on orientation

The long-slit line profile is most dependent on the orientation of the outflow with respect to the observer's line of sight and the orientation of the spectrometer slit. This is true for full slit coverage of the outflow. If the slit does not cover the whole structure, the resulting spectrum is also strongly dependent on the slit position. This dependence is discussed in more detail in Section 3.5. The detailed shape of the outflow and the change in emissivity as a function of distance from the starting point (such as, for instance, a slow decrease in emissivity compared with a constant emissivity) only influence the details of the simulated spectrum and not the gross features. The optical emission is rather sensitive to the temperature and density of the flow, and these change considerably where the outflow turns back and becomes turbulent (Loken et al. 1995). It can therefore be expected that optical emission drops drastically near this point, rendering the eddies very faint or undetectable. Therefore we assume a constant emissivity and velocity along the flow line and a Gaussian transverse emissivity distribution of FWHM $= 0.5r_0$, with a cut-off at position $s = s_f$ along the spiral (which we expect to be near the turning point).

In Fig. 2 we show a series of results for axisymmetric outflows, varying the angle between the axis and the line of sight (left to right) and the orientation with respect to the direction of the spectrometer slit (which covers the whole structure). A non-linear grey-scale is

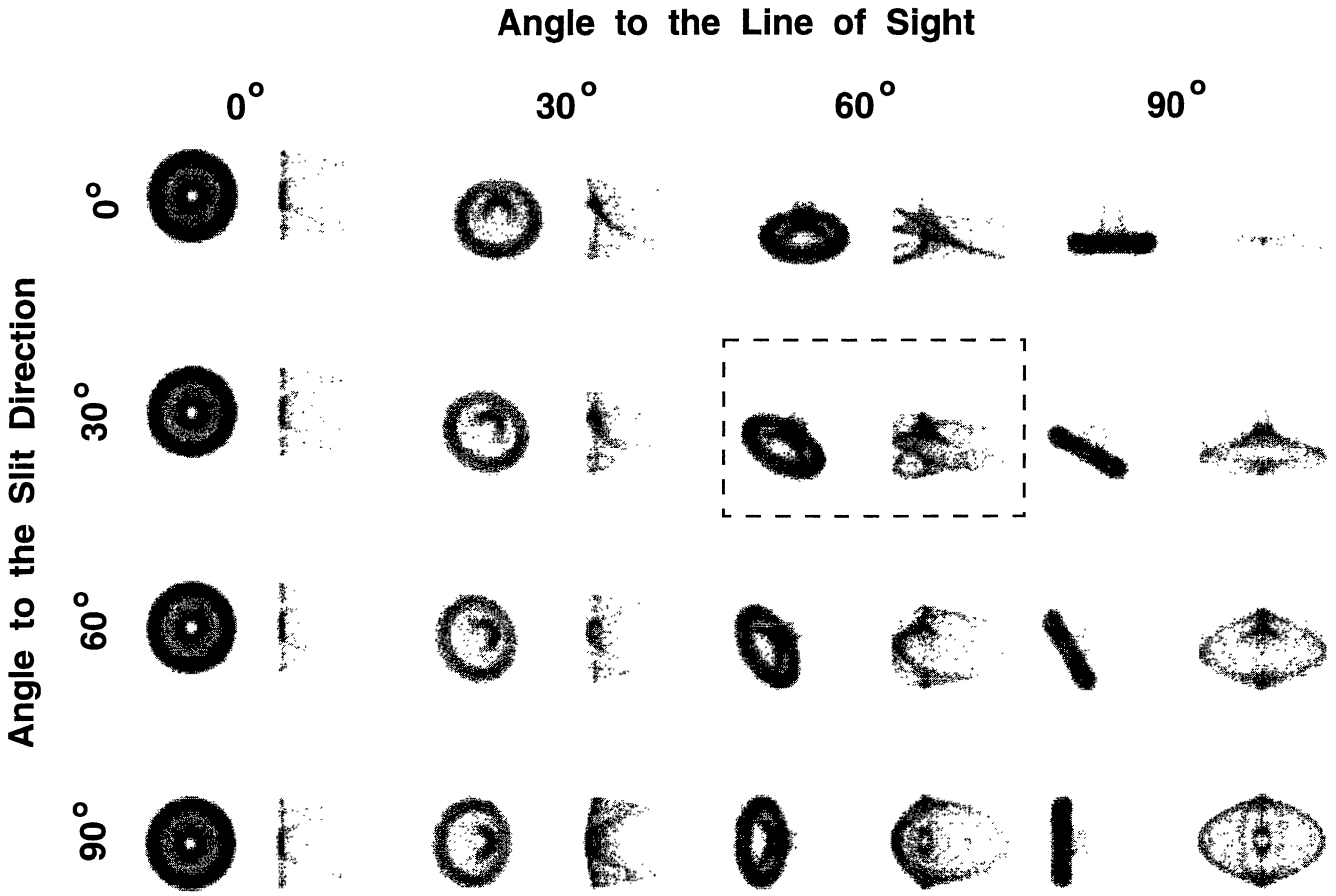

Figure 2. A series of simulations of an opening outflow is shown, varying the orientation of the axis with respect to the line of sight (left to right) and the slit orientation. The slit runs from top to bottom and covers the whole of the emission. Represented are pairs of images (left) and long-slit spectra (right). The simulation marked with a dashed box is shown in more detail in Fig. 3. In this series it is the closest match to the observations at the southern hotspot region in IRAS 04210+0400, and it was used as a starting point for more detailed simulations which are compared with the observations below.

used to emphasize the background emission in the spectra which arises mostly from the eddies. The outflows shown here are directed towards the observer. The emission is therefore mainly blueshifted. Since we are considering only optically thin emission, corresponding orientations away from the observer produce symmetrically redshifted spectra and are omitted. For most orientations the opening section of the outflow produces a bright, asymmetric and opening feature in the spectrum which is often 'Λ'-shaped (or 'V'-shaped, if the outflow is oriented in the opposite direction). The

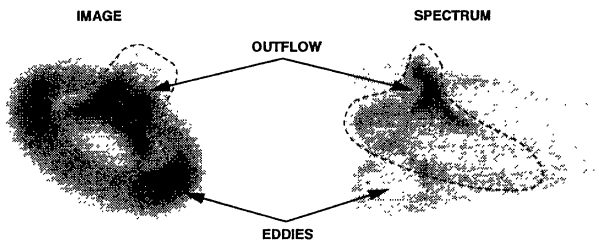

Figure 3. The simulation marked with a dashed line in the previous figure is shown in more detail. The outflowing material, roughly marked with a dashed line in the image simulation (left), basically produces the marked region in the long-slit spectrum (right). Everything outside this region (and some background contribution to the inside region) originates in the backflow and eddy.

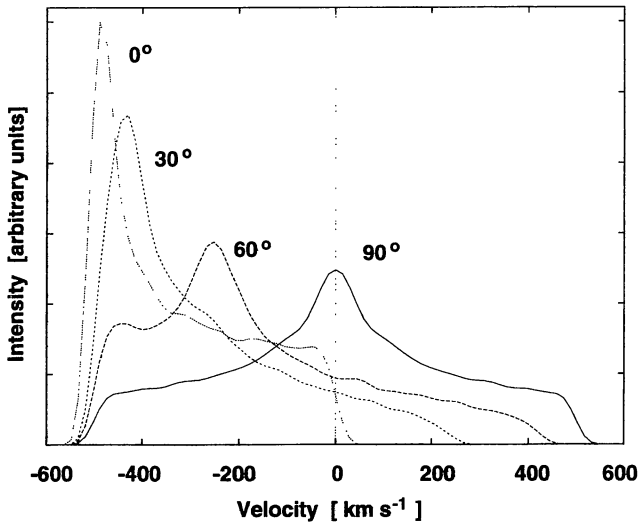

Figure 4. Integrated spectra are plotted which correspond to the long-slit spectra from Fig. 2. Each of the four spectra represents all the long-slit spectra for a particular angle to the line of sight. The four integrated spectra are distinguished by the angle to the slit direction, which is given beside the curves.

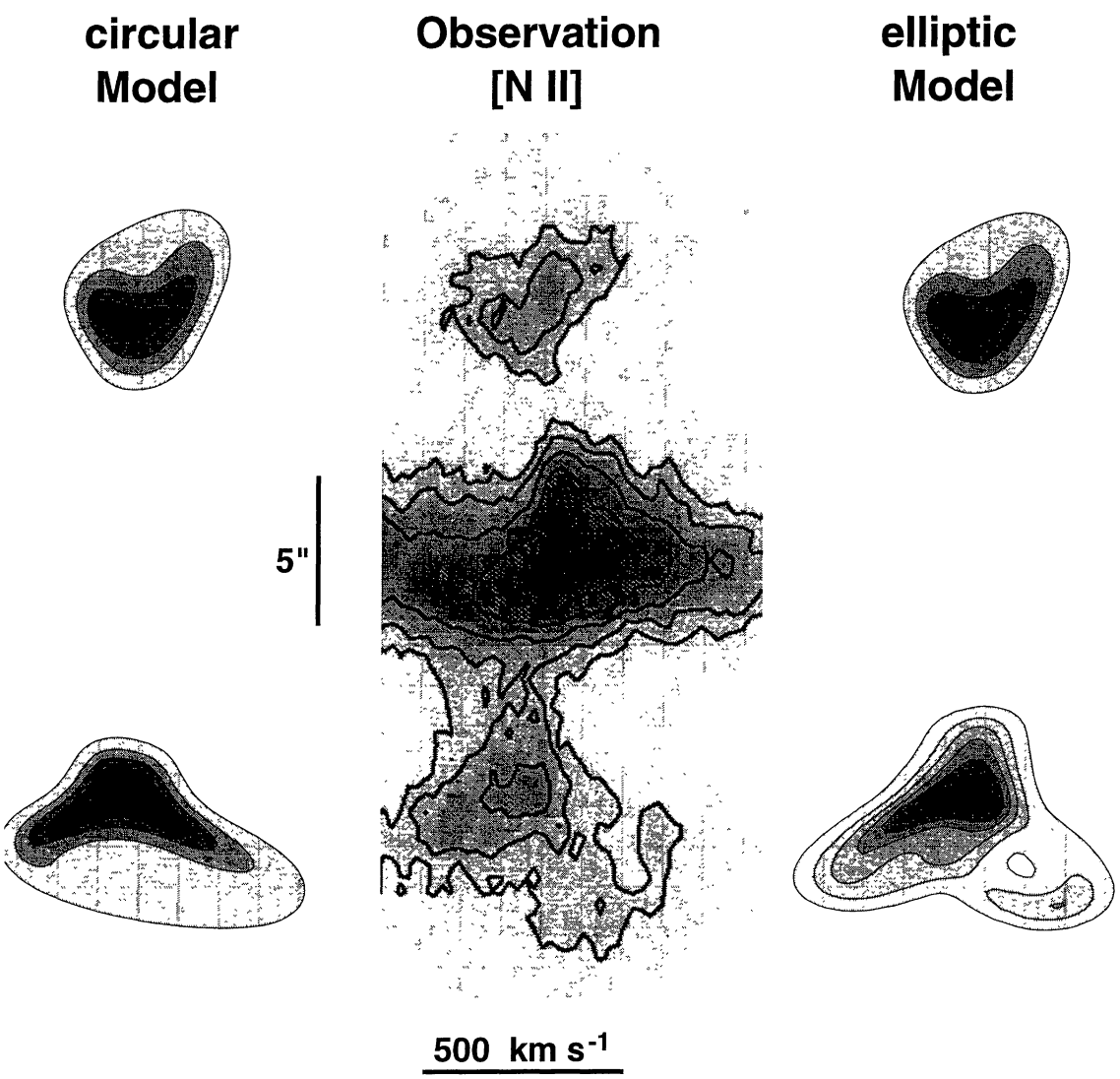

Figure 5. The observed [N II] 6584-Å long-slit spectrum (middle) is compared with our model. On the left the model with the fully circular cross-section is represented. On the right of the observations, the results for the model variant with an elliptic cross-section in the southern outflow are displayed. Observe the flaring of the spectra at approximately 5 arcsec to the north and south of the centre.

eddies generally result in a diffuse distribution around the emission arising from the outflow. The simulation marked with a dashed box in the mosaic (Fig. 2) is shown in detail in Fig. 3 with the outflowing region emphasized with a dashed line. It shows that the back-flow can produce loop-like structures.

In Fig. 4 we display the integrated spectra corresponding to the simulations in the mosaic. Note that the spectra in each column of Fig. 2 have the same shape when integrated. The integrated spectra consist of blueshifted peaks with broad wings mainly from the eddies.

3 OBSERVATIONS

3.1 Long-slit spectra

The long-slit observations to which we apply our model were presented in Paper I, and therefore it will suffice to summarize the main properties that are important for our model. The basic structure can be appreciated best in the [N II] 6584-Å line, which we reproduce in Fig. 5. The northern hotspot at around 5-arcsec separation from the centre shows a 'V'-shaped structure, where the redshifted arm is stronger and more extended.

The southern hotspot shows a very similar 'Λ'-structure, which is better defined: most of the emission spreads into a blue wing. At a lower brightness level, emission is seen in a red wing. The observation is suggestive of two or more discrete components or possibly a ring-like structure in the velocity-space map. A considerably different picture is seen in the [O III] 5007-Å line (reproduced in Fig. 6). Here the 'Λ'-shape is not obvious. Instead, all or most of the emission seems to be in one of the redshifted components also seen in the [N II] 6584-Å line.

As mentioned in Paper I, there are three simple possible kinematic interpretations of such 'Λ'-shaped structures in the velocity map. First, they may arise from real acceleration of the gas. Alternatively, the gas might have a certain high velocity when the line emission starts, and only the direction of the velocity vector changes along its trajectory. Naturally, the third possibility is a combination of both effects. The bifurcations found in the new optical line images presented in the next section provide new evidence for our model of an opening outflow, in which the flaring

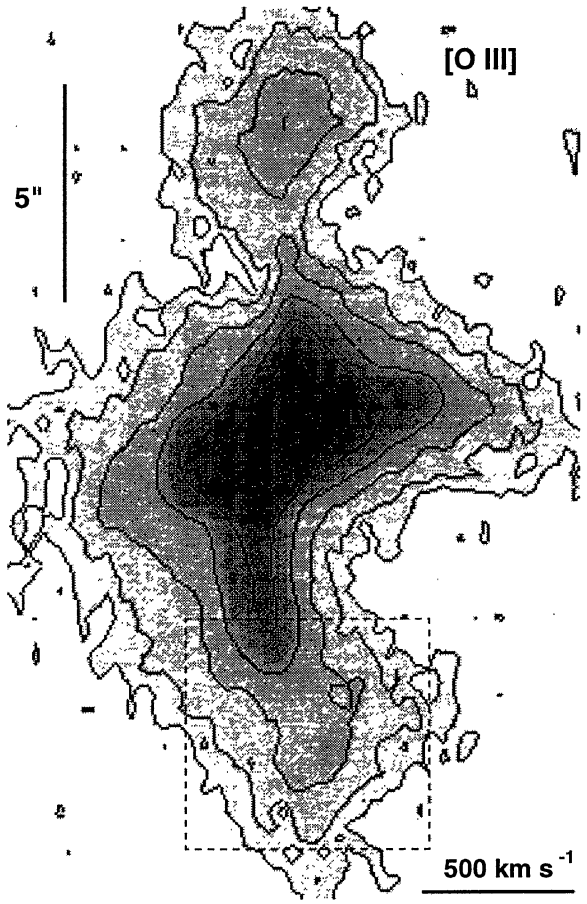

Figure 6. The long-slit profile of the [O III] 5007-Å line (from Paper I). The dashed box marks the southern hotspot region.

of the spectra in the hotspots is dominated by geometric effects (i.e. the flow direction changes along the streamlines).

3.2 New emission-line imaging

In Fig. 7 (opposite p. 1208) we present a new [O III] 5007-Å emission-line image of IRAS 04210+0400. It is a composite of three images of 30-min exposure time each, obtained at the Anglo-Australian Telescope (AAT) with an [O III] 5007-Å filter (bandwidth 70 Å). We show two versions of the same data. In Fig. 7(a) the galaxy is shown, including its near environment, with the grey-scale chosen such that the fainter extended emission is emphasized. In Fig. 7(b) the bright central spiral structure is emphasized. The seeing varied from 1 to 2 arcsec between the individual exposures. The image confirms the central structure observed previously by Beichman et al. (1985). It shows the bifurcation of the 'spiral arm' in the south, which is also present in the *HST* image obtained by Capetti et al. (1996). However, our deep ground-based image clearly reveals a faint bifurcation of the extended emission-line spiral arm beyond the northern hotspot region. This observation strongly supports our interpretation of the flaring of the emission-line width in these regions as an opening outflow of emission-line gas. This northern 'V' is much fainter than the strong bifurcated southern 'arm'.

3.3 Constraints

Before we show the results of detailed models of the observations, we summarize the constraints which can be used as an input for the modelling process. From the new [O III] 5007-Å image, the projected direction (angle Θ) to the axis of the outflow can be estimated from the orientation of the bifurcations. The result is consistent with the orientation of the radio lobes. We find that the approximate position angle of the bifurcations in the north is $-35°$ and in the south is $140°$. Other constraints are the spatial extent and radial velocity width of the emission in the hotspot regions, the asymmetry of the emission in the spectra, and the position of the maximum in the spectra, but these are more difficult to quantify.

The large parameter space has been explored by performing large numbers of intermediate-resolution simulations (≈ 50 pixels along each axis), varying two parameters at a time. The parameter grid was chosen to be fine enough to ensure that only small changes were found between individual frames. The resulting series of images and spectra were inspected, and promising parameter sets were selected and refined. Although a few sets of parameters have been found that reproduce the observations partially, the solutions discussed in the following section give by far the best overall match between the simulation and the observations.

For direct comparison, the simulated images and spectra have been convolved with Gaussian point spread functions with FWHM similar to the resolutions of the observations (with 100 velocity channels).

3.4 Comparison between model and observations

In Figs 5 and 8 we compare the observed long-slit spectrum of the [N II] 6584-Å line and our new [O III] 5007-Å line image, respectively, with our model. The simulation shown on the left is an axisymmetric calculation for both the northern and the southern hotspot region. The important parameters are given in rows 1 and 2 of Table 1. Note that the flaring and the rough brightness distribution in the spectrum are reproduced. However, one does also note that the red wing in the southern hotspot is of similar strength to the blue wing. Also, the maximum emission is within the blue wing. These are general properties of the axisymmetric simulations which fulfil the geometric constraints given in Section 3.3. They are in conflict with the observation.

These problems are solved in the simulation on the right side of Figs 5 and 8. Here the northern model is the same as before, but an elliptic cross-section according to equation (3) was used with an eccentricity of $e = 0.7$. Similarly, the radial velocity component is now $v_{r(\phi)} = v_{r0}\epsilon_{(\phi)}$. Note that the velocity is still constant along each flow line. In this variant of the model, the low-brightness redshifted section of the spectrum (with the shape of a loop) is produced close to the cut-off of the emissivity at s_f. Here the cut-off occurs where the outflow starts to flow back, while in the axisymmetric case the emission cuts off before any back-flow or eddies develop. Note that extending the emission as far as in the elliptic case does not improve the result, but it becomes completely inconsistent with the observation. The loop in the elliptic simulation is similar to the loop in Fig. 3, except that the redshifted emission is now blueshifted and vice versa (since it is pointing away from the observers instead of facing them).

Another improvement of the elliptic model over the axisymmetric case is seen from Table 1. In the axisymmetric simulation, the northern and the southern outflows necessarily have to be pointing towards the observer, i.e. they are not collinear (the angle between their axes is ~155°). In contrast, in the non-axisymmetric simulation the axes form an angle of ~175°, which is consistent with the projected symmetry suggested by the radio lobes.

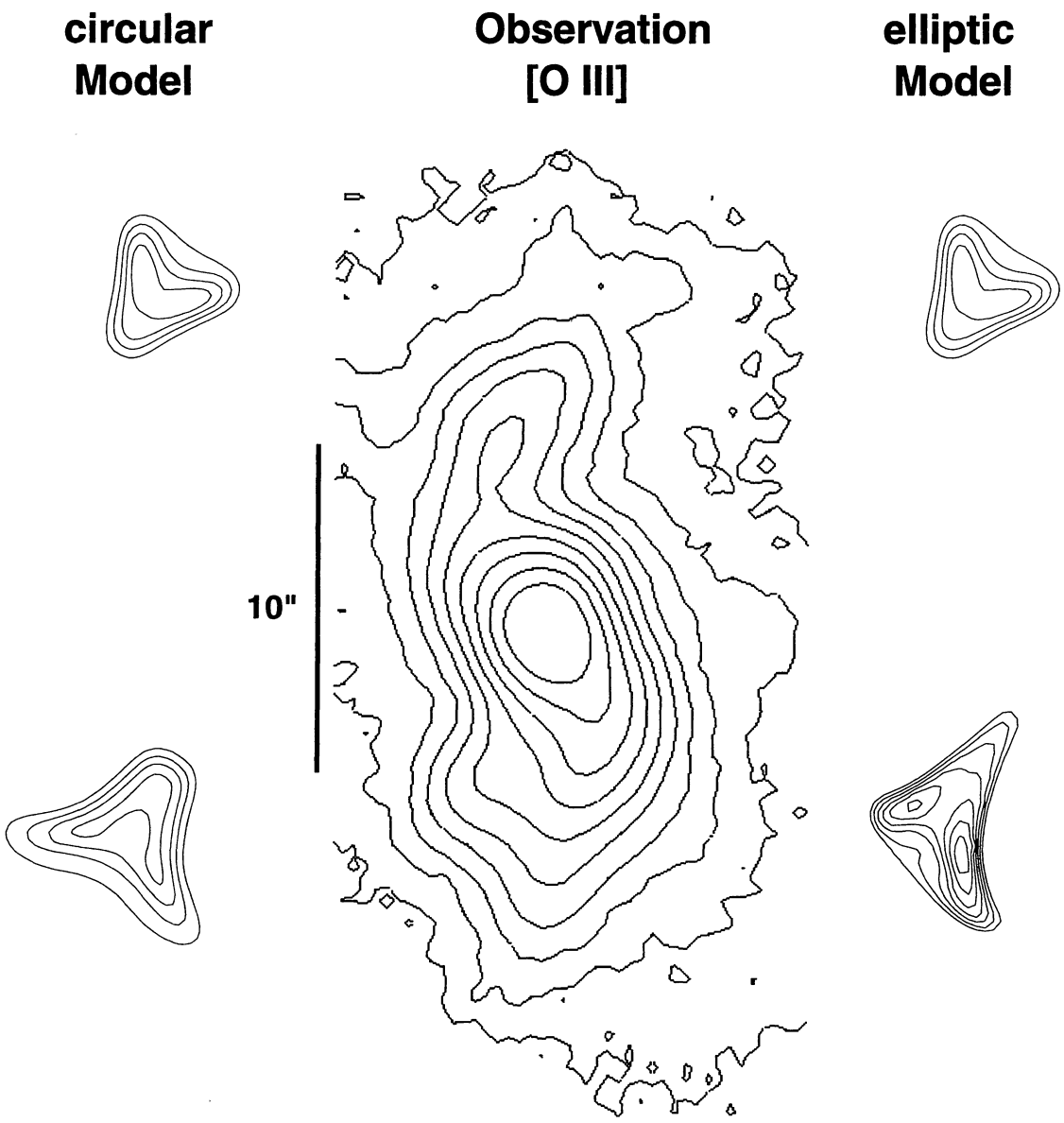

Figure 8. The middle section shows the observed [O III] 5007-Å emission-line image of IRAS 04210+0400. Note the bifurcations to the north and south of the centre, which we identify with the opening outflows. The predicted model images of the flaring regions in the case of an axisymmetric outflow are shown on the left side of the observations. On the right, the simulation in which the southern hotspot region has an elliptic cross-section is represented. Contour levels of the observation are 0.5, 1, 1.5, 3, 6, 10, 15, 25, 40, 60 per cent of the peak brightness. For clarity, the simulated images have equally spaced contours.

Table 1. The geometric parameters and the velocity v of the simulations, which we compare with the observations, are given. The first two rows are axisymmetric simulations of the northern (N) and southern (S) arms. (Θ,Φ,Ψ) are the Euler angles giving the orientation in space with the conventions of Goldstein (1980). Here Θ is the angle with respect to the line of sight and Ψ corresponds to the angle with respect to the slit orientation. The azimuthal orientation of the outflow on the axis is given by Φ. The point at which the emission ceases along the outflow is s_f.

e		v	Θ	Φ	Ψ	b/a	s_f
0	(N)	350	100°	–	35°	0.45	1.7
0	(S)	500	−105°	–	30°	0.8	2.5
0.7	(S)	500	−75°	−35°	35°	0.5	3.2

3.5 Slit coverage and the [O III] 5007-Å line

In this section we consider the effect of slit coverage of the outflow on the appearance of the spectrum. The simulations in the previous section assumed full coverage of the outflow. We note, however, that the size of the slit in the observations was 1 arcsec and the images of the outflows exceed this size in the east–west direction. Another motivation for investigating reduced slit coverage was a significant qualitative difference between the southern hotspot region in the [O III] 5007-Å line and the Hα+[N II] complex. We suspect that this could be due to insufficient slit coverage. As can be seen by comparing Figs 5 and 6, the southern [O III] 5007-Å emission does not show the bright blue- and redshifted wings present in the Hα+[N II] and the [S II] lines at ~5 arcsec from the galaxy centre. A rather discrete redshifted component is present at ~7-arcsec core distance (see Fig. 6).

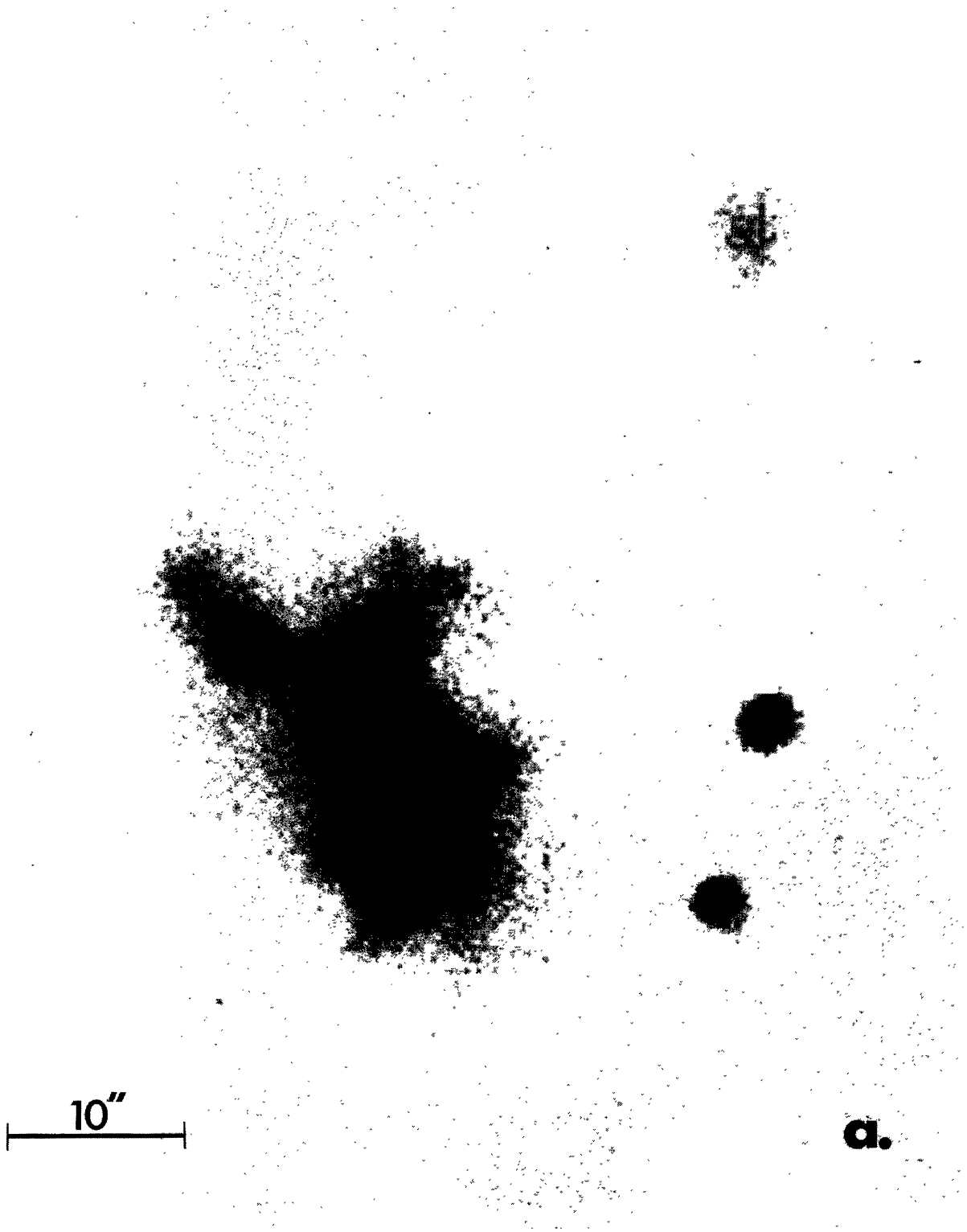

Figure 7. A grey-scale representation of a deep [O III] 5007-Å image taken at the Anglo-Australian Telescope is shown in panel (a), which emphasizes low-brightness features at the edge of IRAS 04210+0400. Note the weak, but clearly detected, bifurcation at the northern edge (north is towards the top). It also shows the near environment which is composed of a small companion galaxy at ~11 arcsec and other barely resolved objects. Unresolved foreground stars are also seen. Panel (b) shows IRAS 04210+0400 only with its companion. The grey-scale was chosen such that the emission-line spiral structure is emphasized.

Figure 7 – *continued*

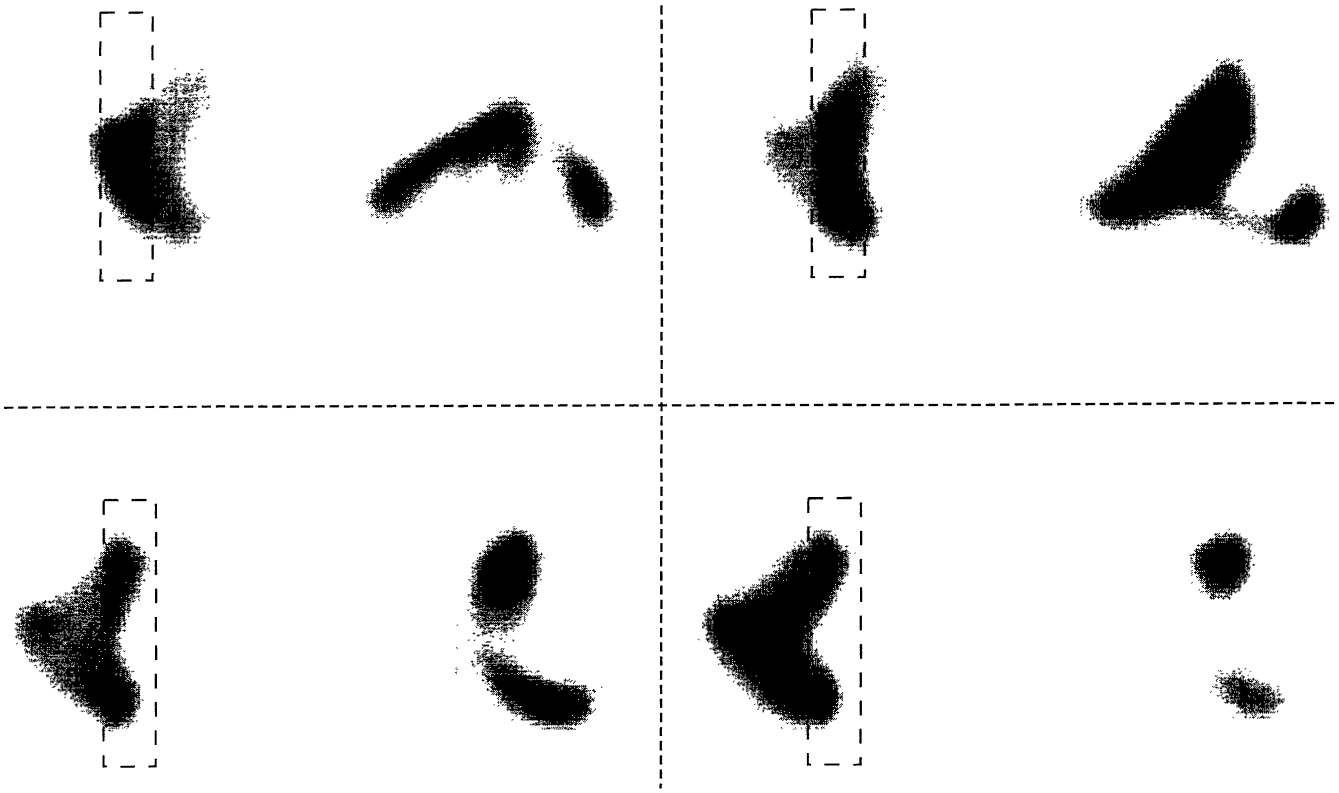

Figure 9. The southern outflow with elliptic cross-section is shown for different slit coverages. As in the previous figures, the pairs of image (left) and long-slit spectrum (right) are shown. The section included in the spectrum is marked by a dashed box and with the intensity enhanced by a factor of 3 in the images.

We consider two possible explanations for this difference. The first of these concerns the uncertainty in the slit coverage of the relevant structures. We note that the Hα+[N II] and [S II] (not all shown here) results are from a single observation, while the [O III] 5007-Å spectrum was obtained on another day and under different seeing conditions. The second possibility is an intrinsic difference in the distribution, possibly caused by the different expansion velocities on a non-axisymmetric opening cone, which could result in different emission properties.

We performed a set of simulations involving a slit that only partially covers the image structures, and stepped it from east to west. We used the non-axisymmetric simulation which compares best with the observations (Fig. 5). In Fig. 9 the area covered by the slit is marked by a box and the brightness is enhanced by a factor of 3 compared with the uncovered portion in the image. As expected, the observed spectrum depends on the slit coverage. However, we also notice that, with the slit covering the central section of the outflow, the upper panels contain all the essential spectral features of the observed Hα+[N II] lines as shown in the simulation with full coverage in Fig. 5. This justifies the reduction of the number of free parameters by choosing full coverage in the simulation of observations with adequate slit positioning.

We also find that inadequate slit coverage could be the reason for the observed difference between the [O III] 5007-Å line and the Hα+[N II] complex. The simulation on the lower right, with the slit covering only small image sections, compares well with the [O III] 5007-Å spectrum. The position of the [O III] 5007-Å feature is reproduced in position and spectral shift. From these considerations we conclude that the difference between the observed [O III] 5007-Å and the corresponding Hα+[N II] emission can be explained by an offset in the positioning of the slit. It probably adequately covers the northern hotspot region, but only partially intersects the southern counterpart. The shift of the slit position corresponds to ~1.5 arcsec and is within the uncertainty of ~2 arcsec from the positioning of the spectrometer slit during the observations.

This result provides the simplest explanation of the difference. However, as discussed in Section 4, it cannot rule out an intrinsic origin of the difference. Note that, in the framework of our model, the [O III] 5007-Å component arises close to the end of the opening cone. A final decision can only be made with further observations with full spectroscopic coverage and detailed physical modelling of the suggested boundary layer between the jet material and the external medium.

4 DISCUSSION

We have considered the kinematics in the extended emission-line region of the active galaxy IRAS 04210+0400. The distribution and kinematics of the emission-line gas seem to be strongly linked to the expansion of extended radio lobes. We have presented a simple model which describes the emission as an opening cone with possible eddies. We have calculated model spectra of such outflows, varying the orientation with respect to the observer's line of sight and the orientation of the spectrometer slit (the most important parameters determining the shape of the long-slit spectra). We find that the main features of the observed long-slit spectra of the extended emission can be explained in terms of two axisymmetric outflows which open very rapidly (over ~1 kpc at a projected distance of ~4.5 kpc).

Both image and spectrum of the northern hotspot region are well described by the axisymmetric model. However, the axisymmetric

case is only of limited use for the southern hotspot region which shows more detailed structure. A significant deviation of the axisymmetric model spectra from the observations of the southern hotspot region is eliminated by allowing for considerable non-axisymmetry of the outflow. Even the simplest possible case, an elliptic cross-section, provides a better match to the observations than the axisymmetric model. Moreover, the predicted image of the elliptic simulation (Fig. 8, right) is in better agreement with our observations and the high-resolution *HST* image presented by Capetti et al. (1996).

From our considerations of the differences between the [O III] 5007-Å and the Hα+[N II] spectra of the southern hotspot region, we find that they could possibly be accounted for by insufficient slit coverage during the [O III] 5007-Å observation. Therefore, re-observation of the [O III] 5007-Å line with adequate coverage and sensitivity is desirable. If the difference is confirmed to be intrinsic, it could provide important information to test a more physical model based on the geometric approach of this paper.

We suggest that the most plausible process producing the morphology and the flow pattern represented by our model is a turbulent mixing layer similar to one described by Cantó & Raga (1991) which could develop rapidly after the jet crossed a shocked boundary between the interstellar and the intergalactic media. However, in contrast to the conditions in their model, which was applied to a supersonic stellar jet, in our case we would have a hot internally subsonic flow, which heavily entrains external gas. This gas is heated and ionized. The temperature will rise from the edge towards the axis, allowing radiation coming from recombination to arise only in a thin sheet close to the edge of the boundary layer. Additional effects could arise from transverse shock waves sent into the external medium as the jet material expands transversely to its main flow direction (Komissarov 1994). At the beginning of the flaring jet region, shock-induced pressure and density of the external gas can be expected to be highest. Coupled with photo-ionization from the centre of the galaxy, this could cause reduced [O III] 5007-Å emission compared with the emission in the region of lower compression further downstream.

The model parameters (Table 1) indicate that the inclination of the axes of the outflows with respect to the plane of the sky is very small (~10°). Hill et al. (1988) suggested that the emission-line spiral structure is due to the residual of the interaction between the jet and the interstellar medium, which then is dragged away from the jet path by rotation. Since the spiral features are observed out to the visible edge of the (disc) galaxy, the jet must have propagated close to the plane of the galaxy in order to encounter sufficiently dense material with which to interact up to the edge of the galaxy. In this case the distance measures along the jet line are largely unaffected by projection effects. If IRAS 04210+0400 is a disc galaxy, the almost circular appearance of the continuum image (Paper I) suggests that it is oriented close to face-on. Unfortunately, the classification of the galaxy is still unclear. In order to settle this question, detailed optical and radio observations will be necessary to separate the effect of the emission-line spiral structure from the starlight and the paths of the jets. The spiral structure and the implications from a model invoking a jet interacting with the external medium have been studied in a separate paper (Steffen et al. 1996b).

5 CONCLUSIONS

We have discussed a simple geometric model of an opening outflow which reproduces the structure found in the long-slit emission-line spectrum of the hotspot regions in IRAS 04210+0400. The predicted optical image structure of these regions is confirmed by deep [O III] line imaging. The model parameters indicate that the axes of the outflows lie very close to the plane of the sky, suggesting that the projected distances along their axes are largely unaffected by projection. We proposed that a jet crossing a shocked boundary between the interstellar and intergalactic media could produce such an outflow in a mixing layer between the jet material and the intergalactic environment. If this model is correct, then IRAS 04210+0400 is a unique object, allowing us to study this phenomenon at optical wavelengths. To date, this has not been possible for the WATs, for which this mechanism has been proposed previously. A more detailed study of this, so far unique, source with the highest possible spatial and spectroscopic resolution and sensitivity is therefore desirable.

ACKNOWLEDGMENTS

AJH and WS acknowledge the receipt of a PPARC studentship and a PPARC research associateship respectively. We thank R.J.R. Williams and A.C. Raga for useful discussions.

REFERENCES

Beichman C. et al., 1985, ApJ, 293, 148
Cantó J., Raga A.C., 1991, ApJ, 372, 646
Capetti A., Axon D.J., Macchetto F., Sparks W., Boksenberg A., 1996, poster presented at IAU Symp. 175, Extragalactic Radio Sources, Bologna, Italy
Goldstein H., 1980, Classical Mechanics, 2nd edn. Addison-Wesley Publishing, Inc., p. 146
Hill G. J., Wynn-Williams C.G., Becklin E.E., MacKenty J.W., 1988, ApJ, 335, 93
Holloway A., Steffen W., Pedlar A., Axon D.J., Dyson J.E., Meaburn J., 1996, MNRAS, 279, 171 (Paper I)
Komissarov S.S., 1994, MNRAS, 266, 649
Loken C., Roettiger K., Burns J.O., Norman M.L., 1995, ApJ, 445, 80
Norman M.L., Burns J.O., Sulkanen M.E., 1988, Nat, 335, 146
O'Donoghue A.A., Eilek J.A., Owen F.N., 1993, ApJ, 408, 428
Owen F.N., O'Dea C.P., Keel W.C., 1990, ApJ, 352, 44
Soifer B.T. et al., 1984, ApJ, 278, L71
Steffen W., Holloway A.J., Pedlar A., Axon D.J., 1996a, in Ekers R., Fanti C., Padrielli L., eds, Proc. IAU Symp. 175, Extragalactic Radio Sources. Kluwer Academic Publishers, Dordrecht, p. 179
Steffen W., Holloway A.J., Pedlar A., 1996b, MNRAS, 282, 130